Electronic Supplementary Material (ESI) for Chemical Communications.
This journal is © The Royal Society of Chemistry 2021

# Supplementary Information

## Quasi-operando quantification of Cu(II) ions in Cu-SSZ-13 catalyst by an $NH_3$ temperature-programmed reduction method

Yue Ma[a,c], Xiaodong Wu[a,*], Jiancai Ding[a], Liping Liu[a], Baofang Jin[a], Eric D. Walter[d], Rui Ran[a], Zhichun Si[b], Feng Gao[c,*] and Duan Weng[a,b,*]

[a] *The Key Laboratory of Advanced Materials of Ministry of Education, School of Materials Science and Engineering, Tsinghua University, Beijing 100084, China*

[b] *Graduate School at Shenzhen, Tsinghua University, Shenzhen 518055, China*

[c] *Institute for Integrated Catalysis, Pacific Northwest National Laboratory, Richland, WA, 99354, USA*

[d] *Environmental Molecular Sciences Laboratory, Pacific Northwest National Laboratory, WA, 99354, USA*

There exist two types of isolated Cu(II) ions in Cu-SSZ-13 under dehydrated conditions,[1] namely $[Cu(OH)]^+$-Z (Z representing negatively charged framework $[Si\text{-}O\text{-}Al]^-$ group) at 8-member ring (8MR) site and $Cu^{2+}$-2Z bonded to 6-member ring (6MR) site, as illustrated by Figs. S1a and S1b, respectively. Note that there are two scenarios for 2Al distribution in one 6MR, namely para-position and meta-position. With a Si/Al ratio of ~12 in the present SSZ-13, most of Al pairs have a para-position configuration,[2, 3] *i.e.*, the case shown in Fig. S1b.

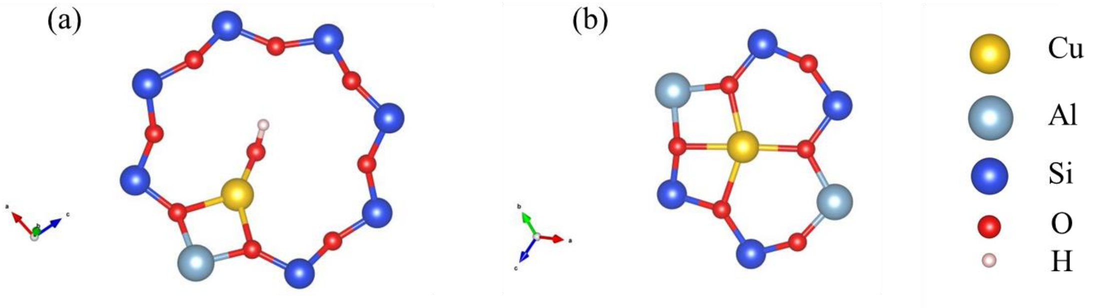

Fig. S1. Scheme of two types of isolated Cu(II) ions in Cu-SSZ-13.

---

[*] Corresponding author. Tel.: +86 10 62792375

E-mail address: wuxiaodong@tsinghua.edu.cn (X. Wu), feng.gao@pnnl.gov (F. Gao),
duanweng@tsinghua.edu.cn (D. Weng).

## Fundamental information of the present SSZ-13 zeolite and Cu-SSZ-13 catalysts

The parent SSZ-13 is a commercial zeolite (H-form) with Si/Al of ~12. Its specific surface area ($S_{\mathrm{BET}}$) and micropore volume (calculated by *t*-plot method) were measured by $N_2$ isothermal adsorption using a JW-BK122F physisorption analyzer (JWGB, China), determined as 707 $m^2/g$ and 0.256 $cm^3/g$, respectively. Cu-SSZ-13 catalysts were prepared by a solution ion-exchange method (*i.e.*, exchanging H-SSZ-13 by $NH_4NO_3$ solution twice to obtain $NH_4$-SSZ-13, followed by exchanging with copper acetate solution at 60 °C). Detailed information of the preparation can be found in our previous work.[4] Cu loading was adjusted by changing copper concentration in solution (0.05-0.2 mol/g) and exchange duration (from 10 min to 4 h). The XRD patterns (collected on a Bruker D8 ADVANCE diffractometer, Germany) of SSZ-13 and Cu-SSZ-13 are shown in Fig. S2, exhibiting only diffraction peaks belonging to CHA structure.

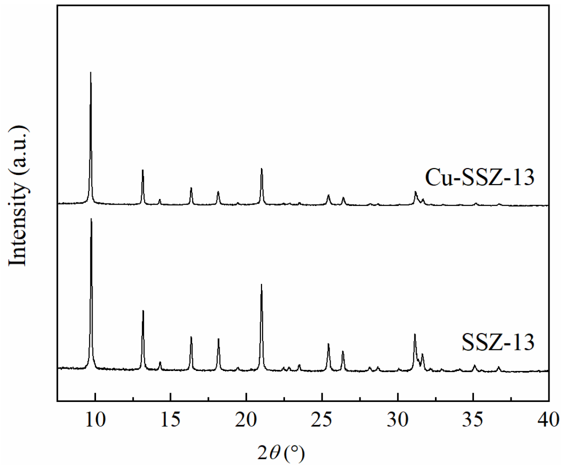

Fig. S2. XRD patterns of the parent SSZ-13 and one of the Cu-SSZ-13 catalysts (with 1.34 wt.% Cu(II) content).

The Cu-SSZ-13 catalyst in Fig. 1 was characterized by $H_2$-TPR on an AutoChem II 2920 chemisorption analyzer (Micromeritics, USA). 100 mg sample was pretreated in 10% $O_2$/He at 300 °C for 30 min in purpose of dehydration and then purged in He at 30 °C to remove residual $O_2$. Afterwards, the catalyst was reduced in 10% $H_2$/Ar (100 mL/min) with a temperature ramp rate of 10 °C/min from 30 to 900 °C. A thermal conductivity detector (TCD) was adopted to measure $H_2$ consumption, and an isopropyl alcohol cold trap (-88 °C) was added upstream of the TCD to condensate water vapor produced from reduction. The result is shown in Fig. S3. The content of isolated Cu(II) ions was determined as 1.34% based on $H_2$ consumption at temperatures lower than 400 ºC. Peak deconvolution indicates the co-existence of $[Cu(OH)]^+$-Z (180 ºC peak) and $Cu^{2+}$-2Z (250 ºC peak) with a ratio of 0.64:0.36.[5]

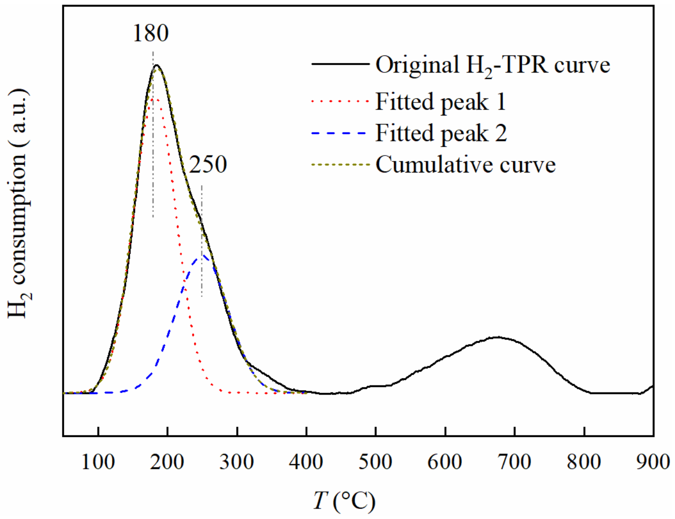

Fig. S3. $H_2$-TPR curve of the Cu-SSZ-13 sample.

To check whether adsorbed $O_2$ in SSZ-13 channels interferes with $NH_3$-TPR, an $O_2$-TPD test was performed over Cu-SSZ-13 (the same as that in Fig. 1). The sample was pretreated in 21% $O_2/N_2$ at 300 ºC for 30 min and then cooled to room temperature in the same gas flow, followed by a purging in Ar. There is almost no $O_2$ desorption (monitored by the MS) at temperatures lower than 400 ºC in Fig. S4 (two orders of magnitude lower than $N_2$ detected in $NH_3$-TPR), implying that $NH_3$ oxidation by adsorbed $O_2$ can be neglected during $NH_3$-TPR. Only a little amount of $O_2$ desorption is observed between 400 and 600 ºC in $O_2$-TPD, attributed to the auto-reduction of $[Cu(OH)]^+$-Z.[6]

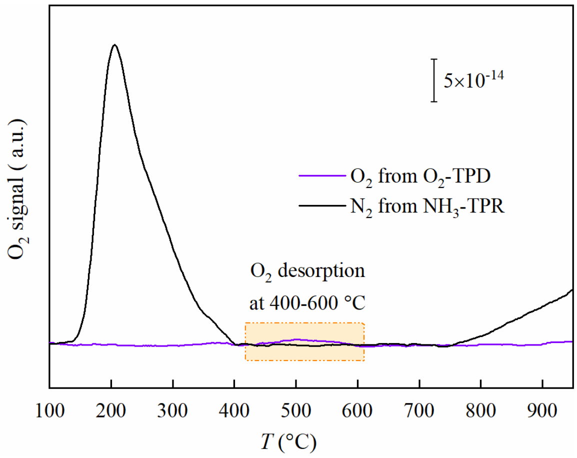

Fig. S4. $O_2$-TPD and $NH_3$-TPR curves of the Cu-SSZ-13 sample.

A mechanical mixture of CuO (25 nm, Meryer, China) and SSZ-13 (with *ca.* 2% Cu loading) was also characterized by $NH_3$-TPR (Fig. S5). A large amount of $N_2O$ is produced over this sample. It is deduced that a high $N_2O/N_2$ ratio in the outlet gas can serve as an indicator for the presence of CuO in Cu-SSZ-13. According to $N_2O$ formation mechanism reported for vanadium-based catalysts,[7] oxidation of $NH_3$ to $N_2O$ by $O_2$ (in the absence of $NO_x$) requires adjacent metal sites and active O species (provided by gaseous $O_2$ and polymeric $V_xO_y$ species) for oxidizing N-H bonds, forming N-O bonds and coupling N-N bonds. Similar mechanism may also work for $NH_3$-TPR of CuO that $NH_3$ adsorbed on adjacent $Cu^{2+}$ is oxidized by active O of CuO to produce $N_2O$. In contrast, such conditions may not be met with isolated Cu(II) ions in ion-exchanged Cu-SSZ-13 (*i.e.*, with long Cu-Cu distance and lack of active bridging O atoms), so $N_2O$ hardly forms.

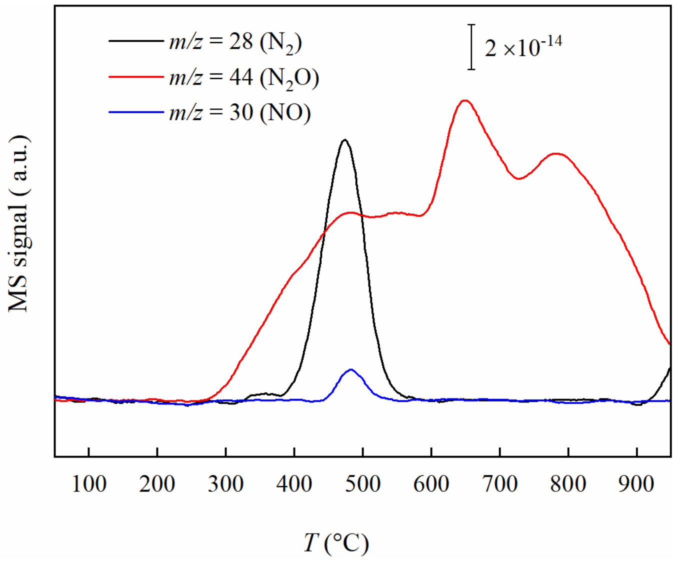

Fig. S5. $NH_3$-TPR curves of the CuO+SSZ-13 mechanical mixture by MS.

$NH_3$-TPR test was also conducted over the parent SSZ-13 zeolite (H-form) for reference (Fig. S6a). Only little amounts of $N_2$ and $N_2O$ were detected at temperatures lower than 700 ºC, probably due to trace amounts of impurities in the parent zeolite. $N_2$ release at temperatures higher than 700 ºC is attributed to thermal decomposition of the inlet $NH_3$.

Cu-SSZ-13 catalyst in Fig. 1 was also reduced by 1% $NH_3$/He (Fig. S6b). $N_2$ release from Cu(II) reduction shifts slightly towards lower temperatures (centered at ~190 ºC) due to the much higher availability of $NH_3$ under this condition, while the total $N_2$ yield below 400 ºC is similar to that in Fig. 1a (using 1000 ppm $NH_3$). Much higher amount of $N_2$ is produced above 600 ºC. This phenomenon demonstrates that high-temperature $N_2$ production mainly arises from $NH_3$ decomposition rather than further reduction of Cu(I) by $NH_3$.

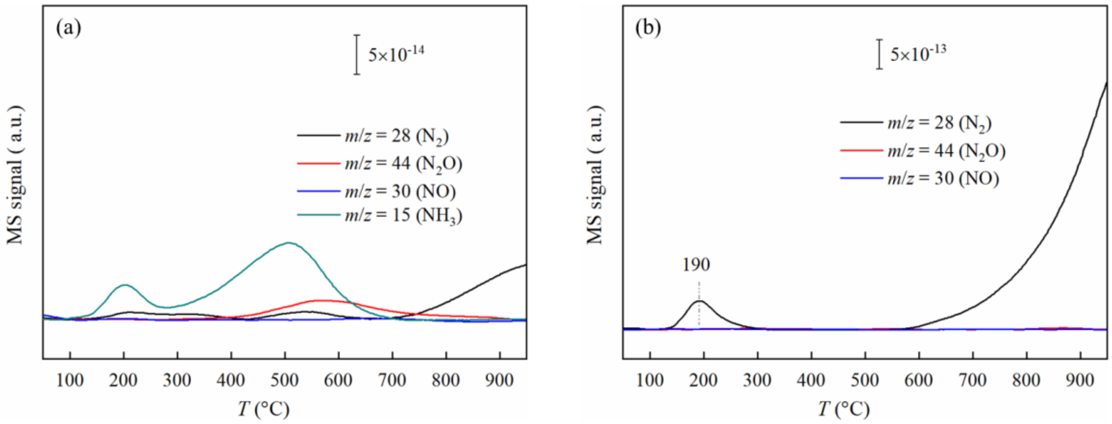

Fig. S6. $NH_3$-TPR curves of (a) SSZ-13 with 1000 ppm $NH_3$/He and (b) Cu-SSZ-13 with 1% $NH_3$/He by MS.

$NH_3$ (using fragment of NH with $m/z = 15$ to avoid interference from $H_2O$) and $H_2$ ($m/z = 2$) signals during the $NH_3$-TPR tests were also monitored by the MS (Fig. S7). Note that a baseline representing 1000 ppm $NH_3$ has been subtracted from the NH curves. Besides, $H_2$ was always detected due to $NH_3$ decomposition in the MS chamber, so a baseline was also subtracted from the $H_2$ curves. Over the parent SSZ-13, additional $H_2$ yield at temperatures between 150 and 700 ºC correlates with its $NH_3$ desorption curve. A larger amount of $H_2$ is detected at temperatures higher than 700 ºC due to decomposition of $NH_3$ in the sample tube. Contrarily, a $H_2$ release peak centered at 235 ºC can be observed over Cu-SSZ-13, which shows a different profile compared with the $NH_3$ desorption curve of this sample but correlates well with its $N_2$ release curve (Fig. 1a). Thus, $H_2$ is demonstrated as a product from the interaction between Cu(II) ions and $NH_3$. Although $H_2$ is as a stronger reductant than $NH_3$, the observed $N_2$/Cu ratio (close to 1:1, almost identical to R4) implies that the reduction of Cu(II) by $H_2$ (RS1) can be neglected. Otherwise, $N_2$/Cu ratio would decrease to lower than 1, *e.g.*, $N_2$/Cu = 0.5 from RS3 ($=\frac{\mathrm{RS1+RS2}}{2}$). The competition between $NH_3$ and $H_2$ may be determined by the presence of excess $NH_3$ in gas phase and adsorbed states (*e.g.*, $NH_3$ on Cu(II) species and $NH_4^+$ on zeolite Brønsted acid sites), which facilitates the Cu(II) reduction by $NH_3$. Therefore, R1, R2 and R4 are determined as the dominant reduction pathways of Cu(II) in $NH_3$-TPR when the Cu(II) content does not exceed 1.66 wt.%.

$$2\mathrm{Cu(II)} + \mathrm{H_2} \rightarrow 2\mathrm{Cu(I)} + 2\mathrm{H^+} \qquad \mathrm{RS1}$$

$$2\mathrm{Cu(II)} + 2\mathrm{NH_3} \rightarrow 2\mathrm{Cu(I)} + 2\mathrm{N_2} + 5\mathrm{H_2} + 2\mathrm{H^+} \qquad \mathrm{RS2}$$

$$(\text{equivalent to } 2 \times \mathrm{R1(or\ R2)} + \mathrm{R4})$$

$$2\mathrm{Cu(II)} + 2\mathrm{NH_3} \rightarrow 2\mathrm{Cu(I)} + \mathrm{N_2} + 2\mathrm{H_2} + 2\mathrm{H^+} \qquad \mathrm{RS3}=\frac{\mathrm{RS1+RS2}}{2}$$

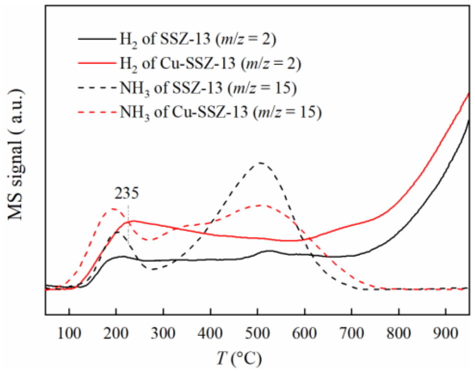

Fig. S7. $H_2$ and $NH_3$ release curves from SSZ-13 and Cu-SSZ-13 during $NH_3$-TPR with 1000 ppm $NH_3$/He.

To investigate the reduction temperature of nitrates, Cu-SSZ-13 was pretreated in 500 ppm $NO_2$/5% $O_2$/$N_2$ at 150 ºC for 1 h in purpose of nitrate deposition.[8] A sharp and intense $N_2$ release peak occurs at ~245 ºC in the following $NH_3$-TPR test (Fig. S8). By comparing with the $N_2$ release curve of air-pretreated sample, the newly developed $N_2$ release feature of the $NO_2$-pretreated sample is obviously attributed to the reduction of stored nitrates on catalyst. The two Cu(II) reduction features (*e.g.*, fitted peaks at *ca.* 205 and 280 ºC, respectively) are not affected by nitrate deposition. The nature of stored nitrates may change with different deposition conditions (*e.g.*, with NO or $NO_2$, in presence/absence of $NH_3$/$O_2$), but all nitrates would transform to similar $NH_4NO_3$-like species during $NH_3$ saturation.[8, 9] So the differently pretreated samples are suggested to share a similar peak position of nitrate reduction in $NH_3$-TPR, and the peak intensity depends on the amount of nitrate deposition. Accordingly, the additional $N_2$ release feature after NO+$NH_3$+$O_2$+$H_2O$ and NO+$NH_3$+$H_2O$ pretreatment is attributed to deposited nitrates during the pretreatments, and the corresponding peak temperature was located at 247 and 253 ºC in deconvolution, respectively (Fig. 3b).

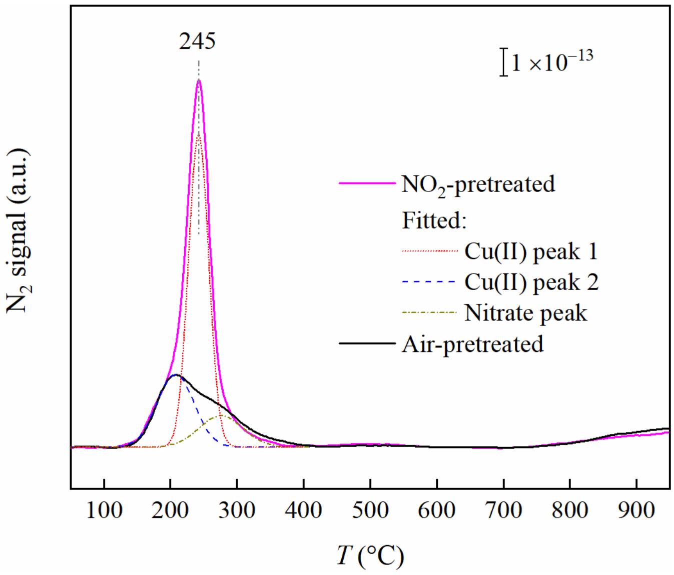

Fig. S8. $NH_3$-TPR curves of Cu-SSZ-13 after pretreatment in 500 ppm $NO_2$/5% $O_2$/$N_2$ or 21% $O_2$/$N_2$ at 150 ºC.

The in-situ EPR spectra of Cu-SSZ-13 during 200 ºC steady-state SCR reaction and after $O_2$ cutoff are shown in Fig. S9, which exhibit typical features of $NH_3$-coordinated Cu(II) ions.[10, 11] Since both $[Cu(OH)]^+$-Z and $Cu^{2+}$-2Z are EPR-active with $NH_3$ coordination,[12] Cu(II) proportion of the catalyst can be determined by EPR signal intensity.

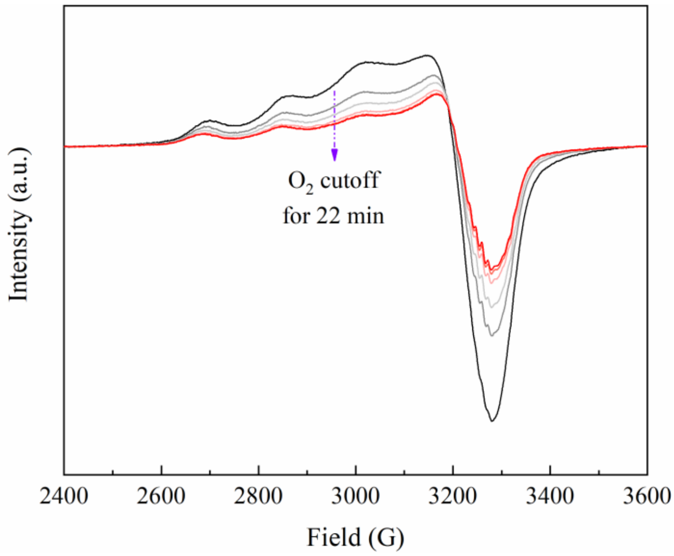

Fig. S9. EPR spectra of Cu-SSZ-13 after being equilibrated in 500 ppm NO/500 ppm $NH_3$/5% $O_2$/3% $H_2O/N_2$ at 200 ºC (black curve), followed by $O_2$ cutoff (grey and pink curves for intermediate states and red curve for steady state after 22 min).

## References

1. C. Paolucci, A. A. Parekh, I. Khurana, J. R. Di Iorio, H. Li, J. D. A. Caballero, A. J. Shih, T. Anggara, W. N. Delgass, J. T. Miller, F. H. Ribeiro, R. Gounder and W. F. Schneider, *J. Am. Chem. Soc.*, 2016, **138**, 6028.
2. F. Gao, N. M. Washton, Y. Wang, M. Kollár, J. Szanyi and C. H. F. Peden, *J. Catal.*, 2015, **331**, 25.
3. J. R. Di Iorio and R. Gounder, *Chem. Mater.*, 2016, **28**, 2236.
4. Y. Ma, X. Wu, S. Cheng, L. Cao, L. Liu, Y. Xu, J. Liu, R. Ran, Z. Si and D. Weng, *Appl. Catal. A*, 2020, **602**, 117650.
5. J. Luo, F. Gao, K. Kamasamudram, N. Currier, C. H. F. Peden and A. Yezerets, *J. Catal.*, 2017, **348**, 291.
6. V. L. Sushkevich and J. A. van Bokhoven, *Chem. Commun.*, 2018, **54**, 7447.
7. M. Yates, J. A. Martín, M. Á. Martín-Luengo, S. Suárez and J. Blanco, *Catal. Today*, 2005, **107-108**, 120.
8. H. Chen, Z. Wei, M. Kollar, F. Gao, Y. Wang, J. Szanyi and C. H. F. Peden, *J. Catal.*, 2015, **329**, 490.
9. A. Grossale, I. Nova and E. Tronconi, *J. Catal.*, 2009, **265**, 141.
10. M. Moreno-González, B. Hueso, M. Boronat, T. Blasco and A. Corma, *J. Phys. Chem. Lett.*, 2015, **6**, 1011.
11. A. Godiksen, O. L. Isaksen, S. B. Rasmussen, P. N. R. Vennestrøm and S. Mossin, *ChemCatChem*, 2018, **10**, 366.
12. Y. Zhang, Y. Peng, J. Li, K. Groden, J. McEwen, E. D. Walter, Y. Chen, Y. Wang and F. Gao, *ACS Catal.*, 2020, **10**, 9410.